Nikparast *et al. Insights into Imaging* (2022) 13:74
https://doi.org/10.1186/s13244-022-01207-6

Insights into Imaging

EDUCATIONAL REVIEW

Open Access

Brain pathological changes during neurodegenerative diseases and their identification methods: How does QSM perform in detecting this process?

Farzaneh Nikparast[1], Zohreh Ganji[1], Mohammad Danesh Doust[1], Reyhane Faraji[1] and Hoda Zare[1,2*]

Abstract

The presence of iron is essential for many biological processes in the body. But sometimes, for various reasons, the amount of iron deposition in different areas of the brain increases, which leads to problems related to the nervous system. Quantitative susceptibility mapping (QSM) is one of the newest magnetic resonance imaging (MRI)-based methods for assessing iron accumulation in target areas. This Narrative Review article aims to evaluate the performance of QSM compared to other methods of assessing iron deposition in the clinical field. Based on the results, we introduced related basic definitions, some neurodegenerative diseases, methods of examining iron deposition in these diseases, and their advantages and disadvantages. This article states that the QSM method can be introduced as a new, reliable, and non-invasive technique for clinical evaluations.

Keywords: Quantitative susceptibility mapping, Alzheimer's disease, Iron, Magnetic susceptibility

*Correspondence: Zareh@mums.ac.ir
[1] Medical Physics Research Center, Mashhad University of Medical Sciences, Mashhad, Iran
Full list of author information is available at the end of the article

Graphical abstract

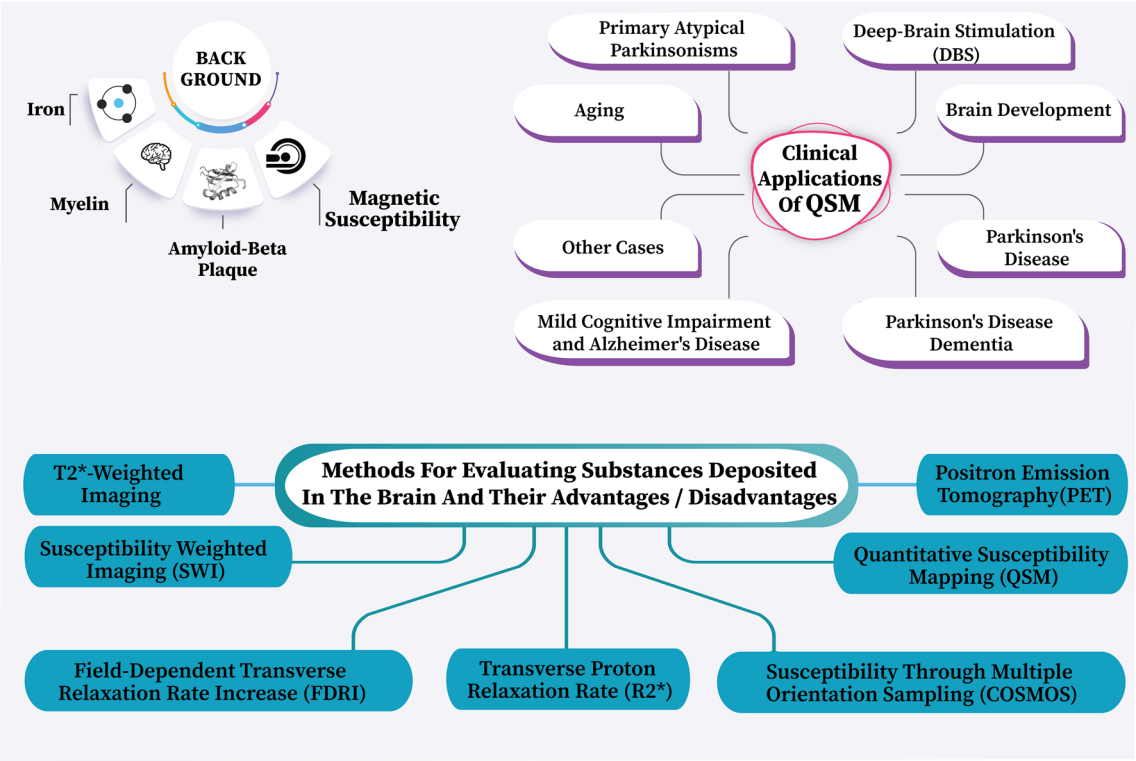

Key points

- Identify the mechanism of the most significant pathological changes in the brain during neurodegenerative diseases.
- Diagnostic imaging methods to identify these pathological changes and the advantages and disadvantages of each.
- The clinical role of QSM and its function in the early detection of neurodegenerative diseases.

Introduction

Iron plays a fundamental role in many biological processes such as cell growth, cell differentiation, protein expression, etc.

Despite the need for iron in the brain, its increase leads to toxic free radicals, oxidative stress, and nerve cell damage [1].

Iron deposition happens in various brain areas in some diseases of the nervous system and the aging process.

There are different imaging methods based on MRI for examining and measuring iron deposition in the brain, like T2*-weighted imaging (T2*WI), T2-weighted imaging(T2WI), relaxation rate (R2*), field-dependent relaxation rate increase (FDRI), and susceptibility-weighted imaging (SWI) [2].

Recently, techniques based on deep learning, machine vision, and medical image processing to diagnose neurodegenerative diseases have expanded; and today, quantitative susceptibility mapping (QSM) is one of the newest medical image post-processing techniques [3–8]. Iron Sediments cause changes in the magnetic susceptibility properties of brain tissue; QSM is a new and non-invasive method that works based on these changes to evaluate the values of iron accumulations.

It is a processing technique that can measure tissue susceptibility from various sequences such as Gradient echo sequences (GRE) and does not have many limitations [9].

This observational-descriptive article explains the main pathological factors in neurodegenerative diseases and how they work and move step by step to diagnostic imaging methods for these pathological factors and their advantages/disadvantages by summarizing the results of different articles.

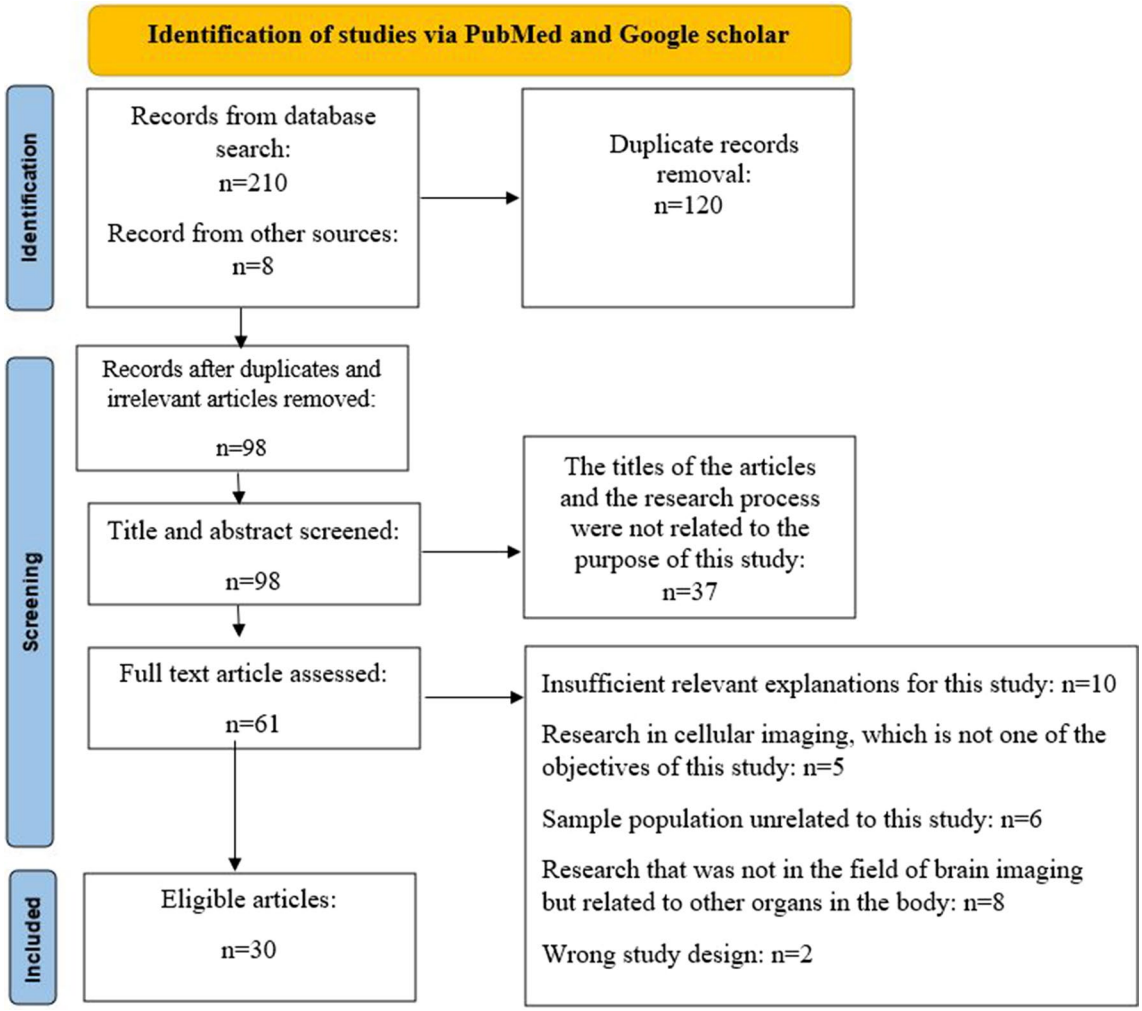

Fig. 1 Follow-up search method based on PRISMA guideline

Finally, a comparison between these methods and the QSM method was performed. This article aims to obtain sufficient information about the first brain changes in the early stages of cognitive disorders and their imaging methods and understand the QSM technique and its clinical applications.

Materials and methods

The Preferred Reporting Items for Systematic Reviews and Meta-Analyses (PRISMA) guidelines were the headline for selecting suitable articles [10] (Fig. 1).

Databases of PubMed and Google Scholar were searched to obtain the relevant articles for this paper.

The keywords used included Quantitative susceptibility mapping, amyloid-Beta PET, Tau PET, Alzheimer's disease, Iron, Magnetic susceptibility, and basal ganglia (BG) from 2013 to 2021.

From the final cases, articles were selected that provided more relevant and complete explanations about the relationship between iron and neurodegenerative diseases and its imaging methods.

Results

Background

Iron

Iron is the most abundant non-diamagnetic element in the human brain, mainly stored as hemosiderin-6 or ferritin in the brain.

It can be transmitted between different brain parts along sections of nerve cells by non-transferrin-bound and transferrin-bound iron forms [11, 12].

Iron plays a crucial role in many biological functions of the body, such as cell growth and differentiation, protein

expression, cyclin accumulation, and the production of reactive oxygen species [1].

Iron acts as a Co-factor for various enzymes involved in functions, such as oxygen transfer, electron transfer, neurotransmitter, and myelin production [13, 14].

Despite all the benefits of having iron in the body, excessive iron levels in the brain are seen in different roles in destroying the nervous system, leading to the production of toxic free radicals, resulting in oxidative damage (Fig. 2).

Toxic free radicals lead to membrane lipid peroxidation and lipofuscin accumulation in nerve cells [1].

Oxidative stress is associated with reducing the function of nerve cells [15] and selective cognitive decline in patients with or without dementia [16].

The presence of iron as one of the main components of senile plaques and neurofibrillary tangles has been proven [17].

In other words, iron concentration is an ideal condition for amyloid-beta (Aβ) aggregation and neurotoxicity [18].

According to a recent study by Ayton et al. [19], there is an association between iron accumulation in the inferior temporal gyrus (ITG) and the slope of cognitive decline in individuals with significant Aβ plaques and neurofibrillary tau tangles.

Excess iron leads to inflammation, which causes a decrease in myelin in the brain [20].

Previous studies have shown that excess iron deposition is closely associated with various neurodegenerative diseases like Alzheimer's and Parkinson's [21].

Iron gradually accumulates in structures such as the BG, hippocampus, cerebellar nucleus, and subcortical areas of the brain [22]; Still, its highest concentration is in deep gray matter (DGM) [23].

Measuring iron deposition in the brain can help explain the pathophysiological process of the disease, be used as a feature in the diagnosis of neurodegenerative disease [24], and basis for targeted treatment [25].

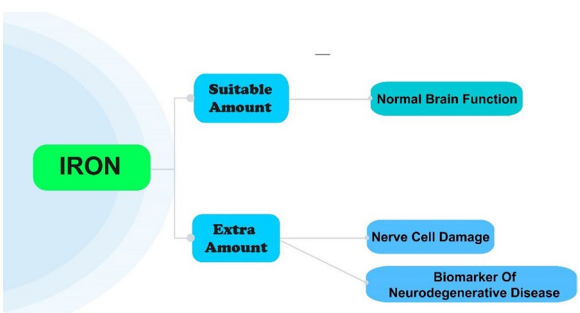

Fig. 2 Consequences of the presence of iron with inappropriate amounts in the brain

We are not yet sure whether iron deposition is the result or cause of neurodegenerative diseases. Still, today we know that monitoring the spatial distribution and temporal dynamics of iron deposition leads to a better understanding of the pathogenesis of the disease [26].

Therefore, quantification of iron deposits is critical; measuring the iron level in different brain parts over specific periods allows us to examine the sequences of disease events.

Myelin

According to the findings, iron is necessary for myelin production, and iron deficiency leads to hypomyelination [11, 20].

Recent studies have reported a negative relationship between iron levels and myelin content in the ventral striatum [27]. However, this relationship needs to be re-examined in the thalamus, BG, and white matter (WM) areas [28].

Myelin degeneration happens in some neurological diseases, such as Alzheimer's disease (AD) and Parkinson's disease (PD), which disrupts iron homeostasis in the brain [29].

However, understanding the relationship between iron concentration and myelin levels in different brain areas, like BG and internal capsule (IC)**,** is necessary to investigate the physiological mechanisms of normal aging and some neurodegenerative diseases.

Amyloid-beta plaque

As mentioned earlier, Aβ deposits are a significant feature of AD.

Proteins generally have high concentrations of paired electrons and are classified diamagnetic materials.

So, the accumulation of Aβ leads to an increase in electron density, changes in local susceptibility, and produces contrast to surrounding natural tissues.

On the other hand, brain iron is a group of paramagnetic substances.

Therefore, Aβ plaques and iron present in the substance have opposite effects on the magnetic susceptibility of the tissue [9].

Magnetic susceptibility

Magnetic susceptibility is an intrinsic and physical property of tissue representing the response of the body's magnetic material to an applied external magnetic field that reflects the composition of the tissue and is used to chemically identify and quantify substances such as iron and calcium and contrast agents [30].

Magnetic susceptibility of the tissue mainly depends on the properties of its content. It is greatly affected by

substances such as iron, lipids, calcium, or myelin in the tissue.

Any change in the concentration and accumulation of these tissue compounds will have consequences.

Iron is the most crucial cause of Magnetic susceptibility changes in subcortical gray matter structures, so it is vital to measure the magnetic susceptibility of these areas of the brain as an indicator of iron deposition in neurodegenerative diseases [31].

Most biological substances, such as calcium or white matter myelin, cause negative susceptibility changes and are diamagnetic.

But iron stored in ferritin, hemosiderin, and neuromelanin in brain tissue, and iron embedded in deoxyhemoglobin in venous blood cause positive susceptibility changes and a strong magnetic field and are classified in the group of paramagnetic materials [32].

Based on the results of previous studies, the amount of iron in the DGM nuclei is well correlated with the magnetic susceptibility of the tissue [33].

Assessing changes in the magnetic susceptibility of brain tissue that occur for various reasons, such as the demyelination process, can give us a good insight into the pathological course of neurodegenerative diseases [34, 35].

The importance of using non-invasive techniques for this assessment is very significant.

Methods for evaluating substances deposited in the brain and their advantages/disadvantages

Over time, different methods for this evaluation have been introduced, each of which has advantages and disadvantages.

There are some imaging techniques; Proton density, T1-weighted, T2-weighted, and T2*-weighted imaging are the routine sequences considered to quantify magnetic susceptibility and indicate the pathological course of the disease [36].

Todays, paramagnetic-deoxyhemoglobin-based fMRI [37], susceptibility weighted imaging [23], phase imaging [16], quantitative susceptibility mapping, and calculation of susceptibility through multiple orientation sampling (COSMOS) technique are used (Figs. 3, 4).

In addition to the methods mentioned, indirect detection of Aβ plaques is possible using MRI methods by injecting a contrast agent such as gadolinium (Gd) or monocrystalline-iron-oxide nanoparticles [38].

T2-weighted imaging*

T2*WI is a new technique based on multi-echo gradient recalled echo (GRE) sequences principles that acquires a gradient echo signal.

This contrast shows changes in tissue susceptibility and thereby creates an assessment of transformations in tissue content.

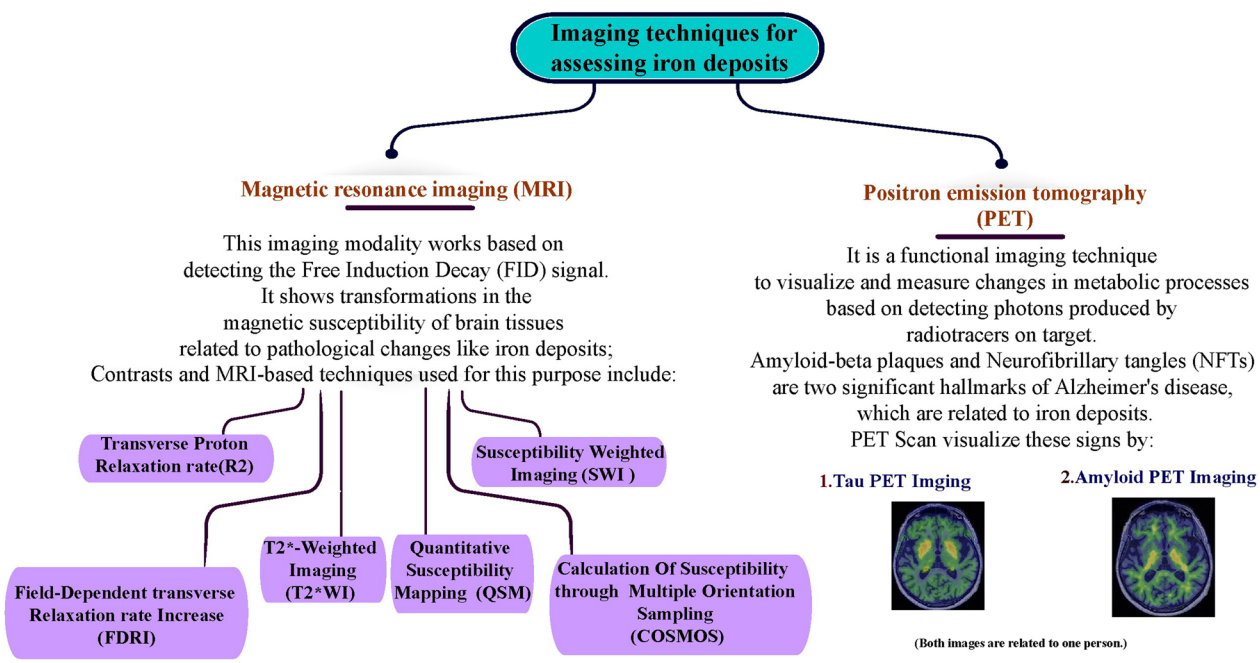

Fig. 3 Methods for evaluating substances deposited in the brain

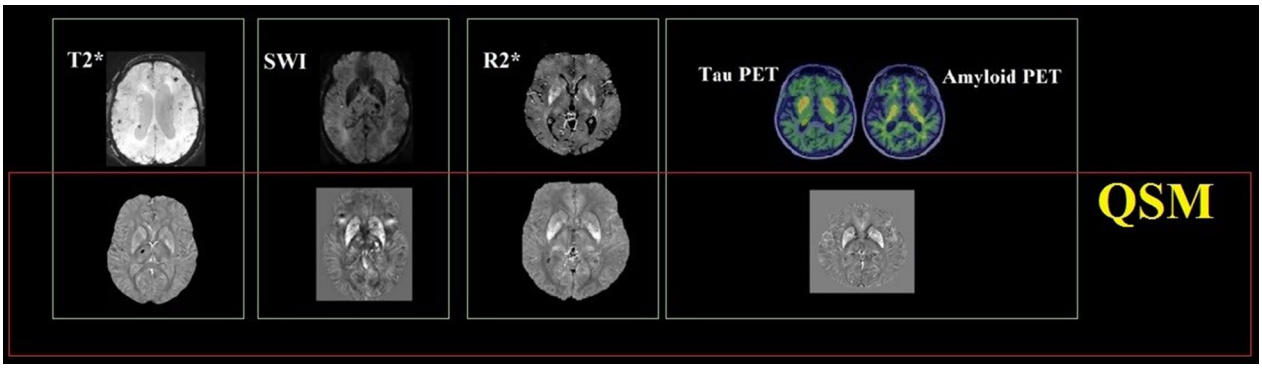

Fig. 4 Presentation of images obtained from some imaging techniques to assess pathological changes in the brain

However, this imaging contrast depends on scanning parameters and object orientation.

Also, its magnitude and phase images contain blooming artifacts [39].

Susceptibility weighted imaging

SWI was introduced by Haacke et al. in 1991.

It is a post-processing strategy that produces susceptibility images obtained only from a single GRE pulse-echo sequence [40] and is the precursor of QSM [41].

This method has many clinical applications, such as cerebral microbleeds examination, hemorrhage, tumor detection, thrombosis, and stroke [42].

Nevertheless, this technique is weak in terms of quantitative validity because the resulting phase is mainly non-local and orientation-dependent. The amount of magnetic susceptibility of the surrounding tissue, the position of the individual's head, and high-pass filtration are some of the factors involved in creating these disadvantages [43, 44].

In addition, SWI images have the blooming artifact, and its quantification is not accurate [45].

Transverse proton relaxation rate

Transverse proton relaxation rate is a non-invasive method used to detect Aβ plaques and is linearly proportional to the amount of iron content [46].

This method can measure the interaction of T2*, which leads to the parameter R2*.

R2∗method suffers from blooming artifacts and cannot measure tissue susceptibility correctly; in addition, results depend on tissue water content, tissue iron content, and scanner field strength [39].

Field-dependent transverse relaxation rate increase

FDRI is one of the first methods for assessing magnetic susceptibility changes of tissue and examining iron deposition in tissues [47].

In this method, R2 imaging performs with two different magnetic field strengths; the increase in relaxation in the higher field is attributed to iron and is a new way to measure iron stores in tissue [48].

This method has limited clinical application because it requires scanning the specified volume with two different magnetic field strengths [49].

Calculation of susceptibility through multiple orientation sampling

Today, a strategy based on a single field strength called the calculation of susceptibility through multiple orientation sampling (COSMOS) has been introduced [50].

COSMOS magnetic susceptibility reconstruction is reliable, but the head needs to be scanned in different orientations [50].

Positron emission tomography

Today, positron emission tomography (PET) scans and radio tracers such as Fluorine-18 based compounds(18F) and carbon-*11*-labeled *Pittsburgh compound B* (*11C*-PIB) are used for in vivo amyloid-beta imaging at preclinical stages [51].

However, drawbacks of PET, including low resolution, high ionizing radiation, and high cost, make it reluctant to use for early screening and early detection of disease [52].

Quantitative susceptibility mapping

QSM is a newfound non-invasive developed MRI technique that can measure the magnetic susceptibility of human tissues [36].

It has the highest specificity and sensitivity for detecting and quantifying iron levels accumulated in the brain compared to other methods; it is possible to study the local tissue magnetic susceptibility property quantitatively [48].

QSM is preferable to the R2* or FDRI methods for evaluating the amount of iron deposition in the brain.

This technique fixes the blooming artifacts, does not depend on echo-time, water content, or field strength, and does not have many limitations mentioned in the previous methods [53, 54].

3D multi-echo gradient echo (mGRE) imaging method is a good sequence for QSM reconstruction [55].

Both phase and magnitude images of the mGRE sequence are used in this technique [48].

Different algorithms of QSM reconstruction steps use phase images to evaluate magnetic susceptibility differences between tissues, detect local variations in iron content, minimize magnetic field orientation dependence, and eliminate non-local effects compared to phase imaging [56].

The four main steps of QSM reconstruction include generating tissue mask, phase unwrapping, background field removal, and field-to-susceptibility inversion; each of which can be performed by different algorithms (Fig. 5).

Quantitative susceptibility mapping disadvantages The execution time of the multi-echo sequences is relatively long; it typically takes 5–10 min for the entire brain scanning, so it is a slow imaging technique.

Keeping the patient's head steady during this time is not an easy task, especially if the patient has a disease such as PD.

Therefore, depending on the patient physical and mental condition, this time is not appropriate for clinical exams [57].

Clinical uses of QSM

The QSM technique to identify pathological changes in the brain has a wide range of applications.

The changes that lead to variances in the magnetic susceptibility of the tissue can be assessed using this technique.

For example, identifying the first brain changes in diseases such as Alzheimer's or Parkinson's, evaluating the process of brain changes during aging, or using this technique to place the relevant electrodes in deep-brain stimulation (DBS) surgery in the correct position, and so on (Fig. 6).

Also, in this section, the routine imaging techniques used in identifying these cases are discussed first. Then the advantages or disadvantages of the QSM technique in the same area are evaluated.

Finally, the proposed differentiation method between the studied groups based on the obtained QSM values is introduced.

After reviewing recent studies, we have listed some critical parameters related to the execution of the MRI imaging sequence required to reconstruct the QSM technique in Table 1.

Deep-brain stimulation

DBS is a reversible stereotactic neurosurgery technique used for PD and other treatment-resistant neurological and psychiatric disorders [58].

Medial globus pallidus (GPm), centromedian nucleus (CM), and the centromedian-parafascicular nucleus complex are the most important goals for DBS [59, 60].

Globus pallidus (GP) separates into the medial globus pallidus (GPm) and the lateral globus pallidus (GPl) by a thin layer called medial medullary lamina (MML) [60, 61].

During the DBS process, electrodes must be located in specific target structures in the brain, then implanted brain pacemaker performs electrical stimulation [62, 63].

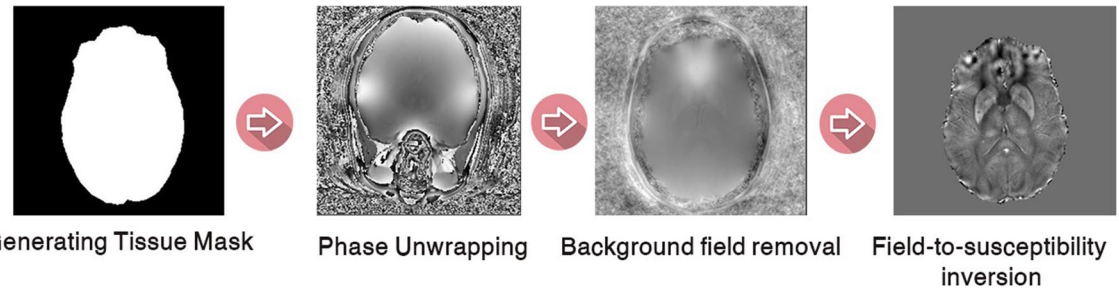

Fig. 5 The four main steps of QSM reconstruction include generating tissue mask, phase unwrapping, background field removal, and field-to-susceptibility inversion

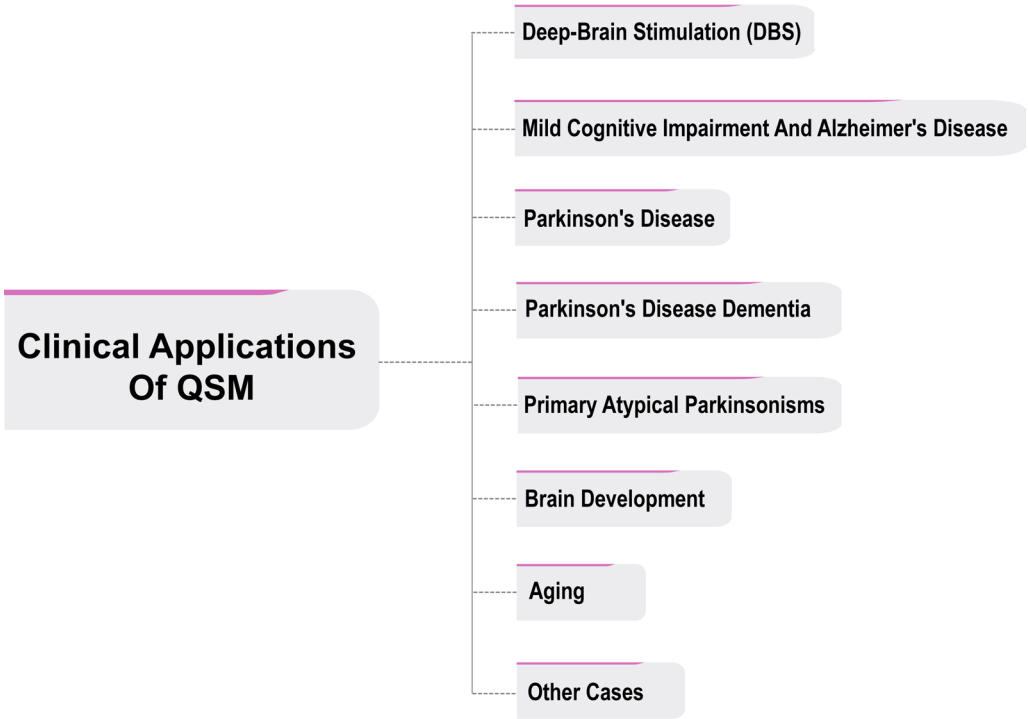

Fig. 6 Clinical applications of QSM

The effectiveness of DBS is related to the ability to accurately target determination because this target is different for each person anatomically [64].

MRI sequences such as T2-weighted fast-spin-echo [65] or proton density-weighted [66] are used to determine the target in DBS and static imaging and obtaining stereotactic imaging data [67].

Some factors cause difficulty to determine the CM coordinates from T1W or T2W images, such as low CM volume [59], lack of sufficient contrast between the CM and the surrounding tissues, so these sequences cannot visualize MML conclusively.

Todays, a normalized atlas is registered to the patient's MRI data to determine the CM coordinates for target localization [68].

The method of indirect targeting uses a normalized atlas which includes limitations because there are differences between the brain structures of different patients, which may lead to registration errors and increase surgical complications [69].

Due to these limitations, the lack of an imaging technique for accurate and direct visualization of CM and GPm makes it hard to target them for DBS surgery.

If the desired anatomical locations are visible with appropriate and specific contrast [70], we can improve the accuracy of the work by direct targeting.

Therefore, it is necessary to have a suitable imaging method to determine and image goals structures [71].

Routine imaging methods used to determine the target structure in DBS High-resolution T1W images with about 14 h of scan time are used to show these substructures of the thalamus, but this method is not suitable for clinical use due to the long scan time [72].

Kanowski et al. showed that using two-dimensional high-resolution proton density-weighted images at 3 Tesla MRI scanners, CM can be identified in 13–26 min. Still, only a few slices covered the target area [73].

Bender et al. showed that by optimized 3D MPRAGE protocol, Relevant doctors could identify CM in 20 min, but thalamic substructures are not well distinguishable [74].

The role of quantitative susceptibility mapping in determining the target structure in this surgery QSM is a reconstructed map of MRI phase images of a three-dimensional multi-echo gradient-echo sequence (3D mGRE).

This magnetic susceptibility map efficiently characterizes brain structures such as the CM region and GPm.

This technique uses magnetic field variations to calculate quantitative maps of magnetic susceptibility changes [71].

Table 1 Demographic information and MRI scans parameters related to research examined research in this study

Study	Sample size	Strength of MRI system	Sequence used	TR	TE
Au et al. [125]	13 Patients with early stage AD, 10 patients with late stage AD, and 30 healthy subjects	3 T	3D fast-field echo	45 ms	8echoes/ΔTE:5.2 ms/ TE1:4.0 ms
Syam et al. [136]	26 Patients with PD, 27 patients with PSP, and 26 healthy subjects	3 T	3D multi-echo gradient-echo	62.2 ms	5 echoes/range 5.7–29.5 ms
Li et al. [132]	114 Healthy subjects	3 T	Gradient echo imaging	53 ms	40 ms
	336 Healthy subjects	3 T		25 ms	17.5 ms
	173 Healthy subjects	1.5 T		25 ms	17.5 ms
Cogswell et al. [126]	296 Healthy subjects, 69 patients with MCI, and 56 patients with amnestic dementia	3 T	3D-MEGRE	28 ms	6.7, 10.6, 14.5,18.4, and 22.4 ms
Fedeli et al. [127]	26 Patients with primary atypical parkinsonisms, and 49 patients with PD	3 T	3D spoiled multi-echo GRE sequences	36 ms	5, 12, 19, 26, and 33 ms
Shahmaei et al. [124]	30 Patients with PD and 15 healthy subjects	3 T	GRE T2*	38 ms	4 and 41.8 ms
Li et al. [122]	22 Patients with AD, 22 Patients with MCI, 25 Patients with SCD, and 25 healthy subjects	3 T	3D multi-echo gradient-echo	41.8 ms	16 echoes/ΔTE: 2.3 ms/TE_1: 3.3 ms
Pu et al. [134]	16 Healthy adult macaques	3 T	3D multi-echo gradient-echo	60 ms	32 echoes/ΔTE = 1.42 ms/ TE_1: 2.4 ms
Spotorno et al. [135]	236 Amyloid-*b*-positive subjects, 78 cognitively unimpaired, and 158 cognitively impaired patients	3 T	3D multi-echo gradient-echo	24 ms	5.00, 8.80, 12.60, 16.40, and 20.20 ms
Spincemaille [139]	10 Healthy subjects	3 T	3D multi-echo gradient-echo	24.48 ms	5 echoes: 3.85, 7.97, 12.09, 16.21, and 20.33 ms
				45.08 ms	10 echoes: 3.85, 7.97, 12.09, 16.21, 20.33, 24.45, 28.57, 32.69, 36.81, and 40.93 ms
		7 T	3D multi-echo gradient-echo	24.55 ms	5 echoes: 3.81, 7.91, 12.00, 16.10, and 20.20 ms
				45.03 ms	10 echoes: 3.81, 7.91, 12.00, 16.10, 20.20, 24.29, 28.39, 32.48, 36.58, and 40.68 ms
Li et al. [131]	10 Healthy subjects	3 T	3D multi-echo gradient-echo	40 ms	6 echoes/ΔTE: 6 ms/TE_1: 6 ms
Gong et al. [92]	4 Pairs of transgenic mice with abnormal beta amyloid-aggregation (Tg-SwDI)	7 T	3D multi-echo gradient-echo	250 ms	TE1: 3.72 ms /ΔTE: 5.52 ms/ TE10: 53.36 ms
Du et al. [2]	30 Patients with AD	3 T	3D gradient-echo (GRE)	22.9 ms	3.2 ms
Li [129]	31 Non-demented PD patients, 10 patients with PDD and 27 healthy subjects	3 T	SWI with velocity-compensated 3D fast-field echo	TR/TE: 28/23 ms	
Kim et al. [121]	19 Patients with aMCI, 19 patients with mild and probable AD, and 19 healthy subjects,	3 T	3D fast field-echo (FFE)	43 ms	TE_1: 3.4 ms/ΔTE: 6.0 ms/ $TE_{7:}$ 39 ms

Table 1 (continued)

Study	Sample size	Strength of MRI system	Sequence used	TR	TE
Wei et al. [140]	7 Healthy subjects	3 T	Standard flow-compensated 3D fast spoiled-gradient-recalled (SPGR)	TR/TE: 50/40 ms	
Ide et al. [128]	19 Patients with PD and 41 healthy subjects	3 T	3D multi-echo spoiled gradient echo (GRE)	58.4 ms	11 echoes/ΔTE: 5 ms/TE_1: 4.5 ms
Moon et al. [133]	12 Patients with VaD, 27 patients with AD, and 18 healthy subjects	3 T	Susceptibility-weighted angiography sequence [SWAN]	37 ms	8echoes/ΔTE: 4.09 ms/ TE_1:3.5 ms
Sun et al. [57]	6 Healthy subjects	1.5 T	Standard gradient recalled echo (GRE) 3D-radiofrequency spoiled GRE	TR/TE: 49/40 ms	
Acosta-Cabronero et al. [21]	8 Patients with early-stage probable AD	3 T	Susceptibility-weighted-imaging	35 ms	20 ms

DBS goal structures such as the subthalamic nucleus and internal Globus pallidus are rich in iron (paramagnetic), and there is white matter (diamagnetic) around them [75–77].

QSM uses the susceptibility differences between contents and has been introduced as a suitable imaging method for CM detection.

Compared to R2* mapping, T2WI, T2*WI, phase imaging, and SWI, QSM images have superior contrast in the visualization of the GPm [78].

Mild cognitive impairment and Alzheimer's disease

Mild cognitive impairment (MCI) is a temporary high-risk stage before the onset of most neurodegenerative diseases [79].

Diagnosis at the MCI stage helps prevent the onset and progression of Alzheimer's disease [80].

AD is part of a large group of neurodegenerative diseases that seriously affect the quality of life of the elderly and impose a heavy economic burden on society.

In recent years, the incidence of AD has been increasing; the two most important clinical features of this disease are cognitive decline [81] and memory loss [82].

Early pathological changes occur in the early stages of the disease. As the disease progresses, symptoms such as learning disabilities and memory impairment develop, and we use clinical criteria to diagnose AD [52].

Today we have concluded that microscopic changes occur long before morphological changes and the onset of clinical signs [83]; introducing a reliable and sensitive biomarker at the microscopic and pathological level is required for early diagnosis and monitoring of disease progression [84].

Due to the lack of a reliable biomarker sensitive to these changes, the probable diagnosis of the disease occurs only in the advanced stages.

In the advanced stages of the disease, we also see morphological changes such as hippocampal atrophy, which can be identified using various MRI techniques [85].

Histochemical, histopathological, and imaging studies proved altered iron metabolism is associated with AD [86].

Senile plaques and tau neurofibrillary tangles are essential factors for developing AD. Aβ40 and Aβ42 are Aβ peptides that are most components of senile plaques commonly present in AD [87].

Today, the relationship between iron accumulation in AD and its association with Aβ aggregates and neurofibrillary tangles has been proven [86].

Based on evidence and studies, high iron levels lead to the overproduction of these Aβ peptides [88]; these peptides accumulate rapidly and form toxic oligomers and fibrils [89].

Consequently, plaque accumulation with accelerated oxidative stress leads to the loss of nerve cells [83].

Iron deposition and demyelination of WM increase magnetic susceptibility in a specific area of the brain [90].

Routine imaging methods used to diagnose Alzheimer's disease Initial identification of brain plaques in Alzheimer's disease is possible with amyloid-beta and tau PET imaging.

Studies on the association between the QSM and the amyloid-beta PET results have shown that hypersusceptibility occurs with age in areas of the cortex and deep gray nuclei [91].

Research projects have also shown differences in QSM values between people with AD and people with cognitive impairment or other conditions that damage the nervous system [25, 92].

Studies based on the simultaneous use of QSM and amyloid-beta PET to determine the association between iron deposition and Aβ accumulation have also been performed in ex-vivo brain samples and in-vivo mouse models and; the results have been acceptable [25, 34, 92].

The role of quantitative susceptibility mapping in the diagnosis of Alzheimer's disease A wide range of neurodegenerative diseases related to demyelination, inflammation, microbleeds, and high iron deposition in the brain can be evaluated using the QSM technique [54].

Recent studies have also linked QSM-measured iron accumulation to cognitive decline and Aβ accumulation [93].

In addition, good linear correlations were observed in the BG iron content and QSM through post-mortem validation by mass spectrometry [94], X-ray emission and fluorescence[33], and Perls iron staining [95].

Parkinson's disease dementia

After AD, Parkinson's disease is the most common progressive neurodegenerative disease [96].

According to previous studies, the BG regulate the onset of motor activity.

A deficiency in the natural inhibition of the BG leads to the symptoms observed in PD [97].

Dopamine is a neurotransmitter [98] and acts in pathways such as the dopaminergic pathway from the substantia nigra (SN) to the caudate (Cd) and putamen (Pt) nuclei.

Abnormal deposition of iron in the deep gray nuclei of PD patients is the cause of dopaminergic neuron cell degeneration in the SN; after that, the production of dopamine stops, and the body's movements become irregular [99].

In the nervous system, α-synuclein is a presynaptic neuronal protein in various brain parts, such as the hippocampus, SN, neocortex, cerebellum, and thalamus.

Its abnormal accumulation in patients with PD leads to the formation of Lewy bodies.

Due to this feature, PD can be considered as a type of synucleinopathies [54].

On the other hand, according to a previous study by Langkammer et al. strong linear relationship was observed between the concentration of iron and the magnetic susceptibility value in the structure of gray matter (GM) [23].

One of the most common early non-motor manifestations of PD is dementia; as the disease progresses, symptoms associated with neurological disorders develop [96].

Dementia in PD may be associated with atrophy because MRI studies have shown structural changes in the amygdala and hippocampus in parkinson's disease dementia (PDD) patients [100].

PDD patients experience significant cognitive decline, including impaired executive function, visual function, attention, structural function, and memory.

Compared to AD, lesser deficits in language functions and more significant deficits in executive functions are observed in PDD [101].

According to the evidence, there is a link between limbic anomalies and symptoms of dementia.

Routine imaging sequences used to diagnose Parkinson's disease dementia Researchers can use various MRI sequences to evaluate the mineralization of DGM and differentiate various neurodegenerative Parkinsonian disorders.

These sequences include R2, R2*, SWI, T2WI, and T2 * WI [93].

In this case, R2* imaging is more sensitive than T2 and T2 * weighted imaging [102].

The quality of the R2* imaging technique depends on the strength of the magnetic field; It has no authentic connection with iron accumulations.

Also, blooming artifact in this method increases with increasing time of echo (TE) [103].

Primary atypical parkinsonisms

Parkinsonism is a nervous system syndrome and has different symptoms such as tremors and instability, slowness of activity, and rigidity of muscles.

Primary *Atypical Parkinsonisms (*APPs) are conditions that have different categories such as Progressive Supranuclear Palsy (PSP), Corticobasal degeneration (CBD), and Multiple System Atrophy(MSA) [104].

PSP is the most typical fatal atypical Parkinsonian disorder with a median survival of around seven years [105].

There is currently no specific treatment for PSP other than symptomatic and supportive therapies, and tau-focused methods may be used in the future [106].

PSP has clinical features similar to diseases such as PD, Frontotemporal Dementia (FTD), and CBD [105, 106].

Today differentiating between PD and APPs is the issue of a challenge due to the similarity of symptoms in the early stages of these diseases [107].

The diagnostic method currently used is made on clinical grounds, and the need for a valid biomarker is required for rapid diagnosis of the disease [104].

Routine imaging sequences used to diagnose primary atypical parkinsonisms The SWI sequence is used to diagnose APPs**,** but it does not accurately distinguish between PD and APPs.

Dorsolateral nigral is known as Nigrosome-1, which is considered a sensitive marker of degenerative parkinsonism; The Nigrosome-1 hyperintensity is lost using the SWI sequence.

Therefore, a reliable biomarker in imaging is essential to differentiate between PD,PDD, APPs, and other movement disorders [108].

The role of quantitative susceptibility mapping in the diagnosis of Parkinson's disease dementia and primary atypical parkinsonisms In Parkinson's disease spectrum, there are different patterns of magnetic susceptibility in deep gray nuclei.

APPs patients can be distinguished from PD patients due to different patterns of iron deposition.

QSM is a non-invasive technique that uses magnetic resonance imaging to detect changes in magnetic susceptibility and quantify the amount of iron deposition in the brain [109].

QSM has higher accuracy than other methods[110]. Strong correlations between QSM values and tissue iron content of DGM structure have been observed by postmortem studies [23].

Brain development

According to Li et al., the WM becomes more diamagnetic as the brain develops, from 1 to 83 years old.

During the early phases of brain development, QSM can be used to monitor loss or delayed myelination.

Magnetic susceptibility anisotropy (MSA) is one of the QSM techniques that measure myelin concentration and progression of myelination in the postnatal brain.

A Rapid decrease in Magnetic susceptibility anisotropy values or no improvement represents different conditions such as dysmenorrhea or hypomyelination disorders [111].

Aging

During the aging process, a gradual increase in the magnetic susceptibility values occurs as a natural physiological process due to iron accumulation and myelin breakdown.

In a recent study on using QSM for evaluating age-related changes, a nonlinear increase of susceptibility with aging was perceived in the globus pallidus, red nucleus (RN), SN, and dentate nucleus (DN).

Also, a linear increase in magnetic susceptibility was observed in structures like Pt and Cd [112].

Other QSM clinical applications

In addition to the above, QSM has other clinical uses such as investigation of iron deposition and susceptibility changes in the WM in neurodegenerative diseases such as FTD, Vascular Dementia (VaD), Huntington's Disease (HD), Wilson's Disease, and motor neuron disease (MND) [77].

This technique is also used in neurovascular disorders fields such as traumatic brain injury (TBI), venous oxygen saturation, inflammatory/demyelination disease, assessing brain tumor due to its differentiation of calcification and hemorrhage[113], cerebellar Ataxia, imaging of traumatic intracranial hemorrhage, and monitoring multiple sclerosis patients without the need for Gd [114].

Other areas of use of this method are the evaluation of tissue function in diseases [115],MR venography, checking cerebral cavernous malformations [116], mapping rate of cerebral metabolic [117], mapping magnetic nanocarrier distribution [118], accurate measurement of liver iron concentration [119] and differentiation diamagnetic materials such as calcium from paramagnetic materials such as iron [120].

The methods of differentiation between the studied groups, based on QSM values

The research projects in this field have only compared the iron deposition in the brain nuclei between the studied groups; by reviewing the articles, an increase in iron deposition in several brain nuclei was observed during some cognitive disorders, which can act as biomarkers to differentiate these disorders (Table 2).

Nevertheless, no specific value has been introduced for differentiation between these groups based on the QSM values of various brain regions and different articles have used different methods to achieve this goal.

In general, the Receiver operating characteristic (ROC) curve analyses can differentiate between healthy individuals and the study group in the QSM technique, which requires appropriate Cut-Off values.

So far, no standard cut-off values have been announced, and researchers can use statistical software such as MedCalc (www.medcalc.org, Ostend, Belgium) [121, 122], Excel, or other ways [123, 124] to achieve this goal.

There are different steps and different algorithms for QSM reconstruction that have been used in various research projects [2, 15, 21, 92, 121–136].

Post mortem confirmation study to assess the validity of QSM technique

In 2012, a study was performed to determine the accuracy of the QSM technique for measuring iron deposits in the brain using the QSM technique and inductively

Table 2 Brain nuclei suffer from increased iron deposition in various cognitive disorders (bold = increase QSM values)

		Caudate nucleus		Putamen nucleus		Hippocampus nucleus		Thalamus nucleus	
		QSM values (ppm)							
Moon et al. [133]	AD ($n=27$)	**0.08344 ± 0.02244 $p=0.002$**		**0.0989 ± 0.03363 $p<0.001$**				0.04176 ± 0.02119	
	VaD ($n=12$)	0.0859 ± 0.01369		0.09481 ± 0.0297				0.03129 ± 0.0151	
	CN ($n=18$)	0.06396 ± 0.01638		0.05848 ± 0.02401				0.03671 ± 0.01895	
Kim et al. [121]	AD ($n=19$)			0.00377 ± 0.002851		**− 0.020649 ± 0.002052 $p=0.0010$**		**− 0.019915 ± 0.002081 $p=0.0060$**	
	aMCI ($n=19$)			0.002047 ± 0.002789		− 0.02655 ± 0.002008		− 0.023543 ± 0.002036	
	CN ($n=19$)			− 0.003238 ± 0.002047		− 0.032943 ± 0.002099		− 0.030153 ± 0.002129	
Du et al. [2]	AD ($n=30$)	**(No quantitative information was provided)**		**(No quantitative information was provided)**					
	CN ($n=30$)								
Li et al. [122]	AD ($n=22$)	**0.046 ± 0.011 P = 0.00**		**0.089 ± 0.024 $p=0.00$**		− 0.022 ± 0.006		0.005 ± 0.013	
	MCI ($n=22$)	**0.044 ± 0.009 P = 0.00**		**0.071 ± 0.013 $p=0.00$**		− 0.020 ± 0.008		0.005 ± 0.013	
	SCD ($n=25$)	**0.037 ± 0.006 $p=0.00$**		**0.063 ± 0.012 $p=0.00$**		− 0.018 ± 0.009		− 0.002 ± 0.011	
	CN ($n=25$)	0.023 ± 0.019		0.031 ± 0.024		− 0.023 ± 0.009		− 0.004 ± 0.011	
Julio Acosta-Cabronero et al. [21]	Early stage probable AD ($n=8$)	**(No quantitative information was provided)**		**(No quantitative information was provided)**					
	CN ($n=11$)								
Tiepolt et al. [91]	AD ($n=10$)	R	L	R	L	R	L	R	L
				0.0047 ± 0.0031	0.0031 ± 0.0041	− 0.0028 ± 0.0045	− 0.0020 ± 0.0046	0.0024 ± 0.0036	0.0029 ± 0.0040
	CN ($n=10$)			0.0613 ± 0.0092	0.0482 ± 0.0052	− 0.0775 ± 0.0070	− 0.0513 ± 0.0072	0.0243 ± 0.0039	0.0328 ± 0.0060
Meineke et al. [141]	Mild-AD ($n=29$)	AD versus HC)difference(							
		0.0392 $p<0.05$	**0.0232 $p<0.05$**		0.8879		0.3689		

Table 2 (continued)

		Caudate nucleus		Putamen nucleus		Hippocampus nucleus		Thalamus nucleus
		QSM values (ppm)						
	MCI ($n=31$)	MCI vs HC)difference(						
		0.6026	0.2065		0.7037		0.4509	
	CN ($n=41$)							
Kan et al. [142]	AD ($n=38$)	**(No quantitative information was provided)**				**(No quantitative i nformation was provided)**		
	CN ($n=36$)							
Shahmaei et al. [124]	PD ($n=30$)	0.153 ± 0.027	0.152 ± 0.022				**0.119 ± 0.012 $p=0.005$**	**0.239 ± 0.021 $p<0.001$**
	CN (n = 15)	0.155 ± 0.011	0.163 ± 0.032				0.108 ± 0.008	0.146 ± 0.026
Syam et al. [136]	PD ($n=26$)	0.042 ± 0.0097	0.0404 ± 0.0111					**0.1108 ± 0.0205 $p=0.007$****
	PSP ($n=27$)	**0.0569 ± 0.0121 $p<0.001$**	**0.0641 ± 0.0186 $p<0.001$**					**0.1443 ± 0.0301 $p<0.001$**
	CN ($n=26$)	0.0408 ± 0.0083	0.0401 ± 0.0118					0.0852 ± 0.0149
Li et al. [129]	PD ($n=31$)					**(No quantitative information was provided)**	**(No quantitative information was provided)**	
	PDD ($n=10$)					**(No quantitative information was provided)**		
	CN ($n=27$)							

		Substantia nigra cleus	Amygdala nucleus	Globus pallidus nucleus
		QSM values (ppm)		
Moon et al. [133]	AD ($n=27$)			0.13863 ± 0.03624
	VaD ($n=12$)			0.13195 ± 0.02112
	CN ($n=18$)			0.12678 ± 0.03244

Table 2 (continued)

		Substantia nigra cleus		Amygdala nucleus		Globus pallidus nucleus	
		QSM values (ppm)					
Kim et al. [121]	AD ($n=19$)			**− 0.019073 ± 0.002293 $p=0.0010$**		0.044097 ± 0.004568	
	aMCI ($n=19$)			− 0.027567 ± 0.002243		0.038721 ± 0.004468	
	CN ($n=19$)			− 0.032889 ± 0.002345		0.03804 ± 0.004672	
Du et al. [2]	AD ($n=30$)						
	CN ($n=30$)						
Li et al. [122]	AD ($n=22$)					**0.084 ± 0.015 $p=0.00$**	
	MCI ($n=22$)					**0.063 ± 0.015 $p=0.00$**	
	SCD ($n=25$)					**0.053 ± 0.012 P = 0.00**	
	CN ($n=25$)					0.033 ± 0.024	
Julio Acosta-Cabronero et al. [21]	Early stage probable AD ($n=8$)			**(No quantitative information was provided)**			
	CN ($n=11$)						
Tiepolt et al. [91]	AD ($n=10$)	R	L	R	L	**R**	**L**
				− 0.0097 ± 0.0073	− 0.0056 ± 0.0063	**− 0.0085 ± 0.0088 $P<0.0001$**	**− 0.0071 ± 0.0116 $P<0.0001$**
	CN ($n=10$)			− 0.0942 ± 0.0089	− 0.0637 ± 0.0111	0.2765 ± 0.0181	0.2929 ± 0.0140
Meineke et al. [141]	Mild-AD ($n=29$)						
						0.8163	
	MCI ($n=31$)						
						0.1110	
	CN ($n=41$)						

Table 2 (continued)

		Substantia nigra cleus	Amygdala nucleus	Globus pallidus nucleus
		QSM values (ppm)		
Kan et al. [142]	AD ($n=38$)		**(No quantitative information was provided)**	
	CN ($n=36$)			
Shahmaei et al. [124]	PD ($n=30$)			**0.247 ± 0.028 $p<0.001$**
	CN ($n=15$)			0.178 ± 0.027
Syam et al. [136]	PD ($n=26$)			0.1075 ± 0.021
	PSP ($n=27$)			**0.135 ± 0.0321 $p=0.004$**
	CN ($n=26$)			0.1058 ± 0.0116
Li et al.[129]	PD ($n=31$)			
	PDD ($n=10$)			
	CN ($n=27$)			

coupled plasma mass spectroscopy of post mortem tissue specimens [54].

Based on the estimated brain tissue density of 1.04 g/cm^3 and the effective number of Bohr magnetons (3.78), the contribution of ferritin paramagnetic to tissue susceptibility was estimated to be approximately 0.00132 ppm * [Fe] at 36.5 °C [137].

Since most of the iron in the brain is bound to ferritin proteins, it can be concluded that magnetic susceptibility is sensitive to changes in the concentration of iron in the human brain [22].

However, some factors confuse the results and can have a detrimental effect on the magnetic sensitivity of the tissue, such as iron in oligodendrocytes, which play a significant role in myelination, the abundance of other trace elements, Substances such as deoxygenated blood, transferrin, hemosiderin, myelin, calcium [71] and orientation dependency of susceptibility [138].

Conclusion

There is a wide range of conditions needed to examine magnetic susceptibility changes in the brain.

Different methods each have advantages and disadvantages, but the QSM technique performs relatively well compared to other methods.

This method can be applied to some routine sequences in an MRI scanner and is independent of the field's shape, echo time, direction, and strength.

It has higher spatial contrast than R2 * and higher sensitivity compared to FDRI.

Considering the review of all methods of measuring and evaluating iron deposition in different brain areas, selecting the QSM method for clinical application is a good choice.

However, more extensive studies are required on the clinical use of this technique.

Abbreviations

3D mGRE: Three-dimensional multi-echo gradient-echo sequence (3D mGRE); Aβ: Amyloid-beta plaques; AD: Alzheimer's disease; APPs: Primary atypical parkinsonisms; BG: Basal ganglia; CBD: Corticobasal degeneration; Cd: Caudate nucleus; CM: CentroMedian nucleus; DBS: Deep-brain stimulation; DGM: Deep gray matter; DN: Dentate nucleus; FDRI: Field-dependent relaxation rate increase; FTD: Frontotemporal dementia; Gd: Gadolinium; GM: Gray matter; GPm: Medial globus pallidus; GPl: Lateral globus pallidus; HD: Huntington's disease; ITG: Lower temporal gyrus; MCI: Mild cognitive impairment; mGRE: Multi-echo gradient echo; MML: Medial medullary lamina; MND: Motor neuron disease; MRI: Magnetic resonance imaging; MSA: Magnetic susceptibility anisotropy; MSA: Multiple system atrophy; PD: Parkinson's disease; PDD: Parkinson's disease dementia; PET: Positron emission tomography; PSP: Progressive supranuclear palsy; Pt: Putamen; QSM: Quantitative susceptibility mapping; R2*: Relaxation rate; RN: Red nucleus; SN: Substantia nigra; SWI: Susceptibility weighted imaging; T1W: T1-Weighted; T1WI: T1-weighted imaging; T2WI: T2-weighted imaging; T2*WI: T2*-weighted imaging; TE: Time of echo; T2*W: T2*-weighted; T2WI: T2-weighted; TBI: Traumatic brain injury; VaD: Vascular dementia; WM: White matter.

Authors' contributions

FN: summarize articles and extract important points and write the article of this review article. ZE: selecting appropriate articles based on the set criteria, reviewing the written article in terms of writing accuracy. MD: graphic design and structural review of the article. RF: assistance in writing parts of the article. HZ: author responsible and supervising the scientific accuracy of the content written in this article. All authors read and approved the final manuscript.

Funding

This research was supported by the Vice-Chancellor for Research Department at Mashhad University of Medical Sciences.

Availability of data and materials

Since this is a review article, it is based on recent research. These researches are included in the references.

Declarations

Ethics approval and consent to participate

Not applicable.

Consent for publication

Not applicable.

Competing interests

There are no relevant financial or non-financial competing interests to report.

Author details

[1]Medical Physics Research Center, Mashhad University of Medical Sciences, Mashhad, Iran. [2]Department of Medical Physics, Faculty of Medicine, Mashhad University of Medical Sciences, Mashhad, Iran.

Received: 16 October 2021 Accepted: 13 March 2022
Published online: 13 April 2022

References

1. Koeppen AH (2003) A brief history of brain iron research. J Neurol Sci 207(1–2):95–97
2. Du L, Zhao Z, Cui A et al (2018) Increased iron deposition on brain quantitative susceptibility mapping correlates with decreased cognitive function in Alzheimer's disease. ACS Chem Neurosci 9(7):1849–1857
3. Bigham B, Zamanpour SA, Zemorshidi F, Boroumand F, Zare H (2020) Identification of superficial white matter abnormalities in Alzheimer's disease and mild cognitive impairment using diffusion tensor imaging. J Alzheimer's Dis Rep 4(1):49–59
4. Faraj R, Khandan Khademreza Z, Sharifian S, Zare H (2021) Evaluation of white matter tracts in autistic individuals: a review of diffusion tensor imaging studies. SSU J 29(3):3539–3555
5. Ganji Z, Hakak MA, Zamanpour SA, Zare H (2021) Automatic detection of focal cortical dysplasia type II in MRI: is the application of surface-based morphometry and machine learning promising? Front Hum Neurosci 15:608285
6. Zare H, Zemorshidi F, Sigari MH, Zamanpour SA (2019) Automatic detection of Alzheimer's disease using diffusion tensor imaging and machine vision. Mashhad University of Medical Sciences, Mashhad
7. Zare H, Montazerabadi A, Zemorshidi F, Ghaemmaghami A (2021) Diagnosis of Parkinson's disease and prediction of its clinical indicators with rest functional magnetic resonance images (rs-fMRI). Mashhad University of Medical Sciences, Mashhad
8. Zare H, Khandan Khademreza Z (2020) Diagnosis of autism spectrum disorder and prediction of its clinical indicators with structural magnetic resonance images (sMRI) and rest functional magnetic resonance images (rs-fMRI) using machine vision. Iran, Mashhad: Mahshad University of Medical Sciences (MUMS)
9. Babaei M, Jones IC, Dayal K, Mauter MS (2017) Computing the diamagnetic susceptibility and diamagnetic anisotropy of membrane proteins from structural subunits. J Chem Theory Comput 13(6):2945–2953

10. Shamseer L, Moher D, Clarke M et al (2015) Preferred reporting items for systematic review and meta-analysis protocols (PRISMA-P) 2015: elaboration and explanation. BMJ 2015:349
11. Mills E, Dong XP, Wang F, Xu H (2010) Mechanisms of brain iron transport: insight into neurodegeneration and CNS disorders. Future Med Chem 2(1):51–64
12. Wang Z, Zeng YN, Yang P et al (2019) Axonal iron transport in the brain modulates anxiety-related behaviors. Nat Chem Biol 15(12):1214–1222
13. Moos T, Morgan EH (2004) The metabolism of neuronal iron and its pathogenic role in neurological disease: review. Ann N Y Acad Sci 1012:14–26
14. Zecca L, Youdim MB, Riederer P, Connor JR, Crichton RR (2004) Iron, brain ageing and neurodegenerative disorders. Nat Rev Neurosci 5(11):863–873
15. Bilgic B, Pfefferbaum A, Rohlfing T, Sullivan EV, Adalsteinsson E (2012) MRI estimates of brain iron concentration in normal aging using quantitative susceptibility mapping. Neuroimage 59(3):2625–2635
16. Ghadery C, Pirpamer L, Hofer E et al (2015) R2* mapping for brain iron: associations with cognition in normal aging. Neurobiol Aging 36(2):925–932
17. Good PF, Perl DP, Bierer LM, Schmeidler J (1992) Selective accumulation of aluminum and iron in the neurofibrillary tangles of Alzheimer's disease: a laser microprobe (LAMMA) study. Ann Neurol 31(3):286–292
18. Leskovjan AC, Kretlow A, Lanzirotti A, Barrea R, Vogt S, Miller LM (2011) Increased brain iron coincides with early plaque formation in a mouse model of Alzheimer's disease. Neuroimage 55(1):32–38
19. Ayton S, Wang Y, Diouf I et al (2020) Brain iron is associated with accelerated cognitive decline in people with Alzheimer pathology. Mol Psychiatry 25(11):2932–2941
20. Ward RJ, Zucca FA, Duyn JH, Crichton RR, Zecca L (2014) The role of iron in brain ageing and neurodegenerative disorders. Lancet Neurol 13(10):1045–1060
21. Cardenas-Blanco A, Arnold RJ, Lupson V, Nestor PJ (2013) In vivo quantitative susceptibility mapping (QSM) in Alzheimer's disease. PLoS One 8(11):e81093
22. Hallgren B, Sourander P (1958) The effect of age on the non-haemin iron in the human brain. J Neurochem 3(1):41–51
23. Haacke EM, Cheng NY, House MJ et al (2005) Imaging iron stores in the brain using magnetic resonance imaging. Magn Reson Imaging 23(1):1–25
24. Brass SD, Chen NK, Mulkern RV, Bakshi R (2006) Magnetic resonance imaging of iron deposition in neurological disorders. Top Magn Reson Imaging 17(1):31–40
25. van Bergen JMG, Li X, Quevenco FC et al (2018) Simultaneous quantitative susceptibility mapping and Flutemetamol-PET suggests local correlation of iron and β-amyloid as an indicator of cognitive performance at high age. Neuroimage 174:308–316
26. Schenck JF, Zimmerman EA (2004) High-field magnetic resonance imaging of brain iron: birth of a biomarker? NMR Biomed 17(7):433–445
27. Steiger TK, Weiskopf N, Bunzeck N (2016) Iron level and myelin content in the ventral striatum predict memory performance in the aging brain. J Neurosci 36(12):3552–3558
28. Hametner S, Endmayr V, Deistung A et al (2018) The influence of brain iron and myelin on magnetic susceptibility and effective transverse relaxation—a biochemical and histological validation study. Neuroimage 179:117–133
29. Hadzhieva M, Kirches E, Mawrin C (2014) Review: iron metabolism and the role of iron in neurodegenerative disorders. Neuropathol Appl Neurobiol 40(3):240–257
30. Reichenbach JR (2012) The future of susceptibility contrast for assessment of anatomy and function. Neuroimage 62(2):1311–1315
31. Lim IA, Faria AV, Li X et al (2013) Human brain atlas for automated region of interest selection in quantitative susceptibility mapping: application to determine iron content in deep gray matter structures. Neuroimage 82:449–469
32. Zhong K, Ernst T, Buchthal S, Speck O, Anderson L, Chang L (2011) Phase contrast imaging in neonates. Neuroimage 55(3):1068–1072
33. Sun H, Walsh AJ, Lebel RM et al (2015) Validation of quantitative susceptibility mapping with Perls' iron staining for subcortical gray matter. Neuroimage 105:486–492
34. Hagemeier J, Zivadinov R, Dwyer MG et al (2018) Changes of deep gray matter magnetic susceptibility over 2 years in multiple sclerosis and healthy control brain. NeuroImage Clin 18:1007–1016
35. Schweser F, Raffaini Duarte Martins AL, Hagemeier J et al (2018) Mapping of thalamic magnetic susceptibility in multiple sclerosis indicates decreasing iron with disease duration: a proposed mechanistic relationship between inflammation and oligodendrocyte vitality. Neuroimage 167:438–452
36. Haacke EM, Liu S, Buch S, Zheng W, Wu D, Ye Y (2015) Quantitative susceptibility mapping: current status and future directions. Magn Reson Imaging 33(1):1–25
37. Vaughan JT, Garwood M, Collins CM et al (2001) 7T vs 4T: RF power, homogeneity, and signal-to-noise comparison in head images. Magn Reson Med 46(1):24–30
38. Poduslo JF, Wengenack TM, Curran GL et al (2002) Molecular targeting of Alzheimer's amyloid plaques for contrast-enhanced magnetic resonance imaging. Neurobiol Dis 11(2):315–329
39. Li J, Chang S, Liu T et al (2012) Reducing the object orientation dependence of susceptibility effects in gradient echo MRI through quantitative susceptibility mapping. Magn Reson Med 68(5):1563–1569
40. Haacke EM, Xu Y, Cheng YC, Reichenbach JR (2004) Susceptibility weighted imaging (SWI). Magn Reson Med 52(3):612–618
41. Haacke EM, Lai S, Yablonskiy DA, Lin W (1995) In vivo validation of the bold mechanism: A review of signal changes in gradient echo functional MRI in the presence of flow. Int J Imaging Syst Technol 6(2–3):153–163
42. Mittal S, Wu Z, Neelavalli J, Haacke EM (2009) Susceptibility-weighted imaging: technical aspects and clinical applications, part 2. AJNR Am J Neuroradiol 30(2):232–252
43. Walsh AJ, Wilman AH (2011) Susceptibility phase imaging with comparison to R2 mapping of iron-rich deep grey matter. Neuroimage 57(2):452–461
44. Schäfer A, Wharton S, Gowland P, Bowtell R (2009) Using magnetic field simulation to study susceptibility-related phase contrast in gradient echo MRI. Neuroimage 48(1):126–137
45. Haacke EM, Mittal S, Wu Z, Neelavalli J, Cheng YC (2009) Susceptibility-weighted imaging: technical aspects and clinical applications, part 1. AJNR Am J Neuroradiol 30(1):19–30
46. Meadowcroft MD, Connor JR, Smith MB, Yang QX (2009) MRI and histological analysis of beta-amyloid plaques in both human Alzheimer's disease and APP/PS1 transgenic mice. J Magn Reson Imaging JMRI 29(5):997–1007
47. Bartzokis G, Aravagiri M, Oldendorf WH, Mintz J, Marder SR (1993) Field dependent transverse relaxation rate increase may be a specific measure of tissue iron stores. Magn Reson Med 29(4):459–464
48. Wang Y, Liu T (2015) Quantitative susceptibility mapping (QSM): decoding MRI data for a tissue magnetic biomarker. Magn Reson Med 73(1):82–101
49. Bartzokis G, Sultzer D, Cummings J et al (2000) In vivo evaluation of brain iron in Alzheimer disease using magnetic resonance imaging. Arch Gen Psychiatry 57(1):47–53
50. Liu T, Spincemaille P, de Rochefort L, Kressler B, Wang Y (2009) Calculation of susceptibility through multiple orientation sampling (COSMOS): a method for conditioning the inverse problem from measured magnetic field map to susceptibility source image in MRI. Magn Reson Med 61(1):196–204
51. Klunk WE, Engler H, Nordberg A et al (2004) Imaging brain amyloid in Alzheimer's disease with Pittsburgh compound-B. Ann Neurol 55(3):306–319
52. Gong NJ, Chan CC, Leung LM, Wong CS, Dibb R, Liu C (2017) Differential microstructural and morphological abnormalities in mild cognitive impairment and Alzheimer's disease: Evidence from cortical and deep gray matter. Hum Brain Mapp 38(5):2495–2508
53. de Rochefort L, Liu T, Kressler B et al (2010) Quantitative susceptibility map reconstruction from MR phase data using Bayesian regularization: validation and application to brain imaging. Magn Reson Med 63:194

54. Langkammer C, Schweser F, Krebs N et al (2012) Quantitative susceptibility mapping (QSM) as a means to measure brain iron? A post mortem validation study. Neuroimage 62(3):1593–1599
55. Langkammer C, Pirpamer L, Seiler S et al (2016) Quantitative susceptibility mapping in Parkinson's disease. PLoS One 11(9):e0162460
56. Marques JP, Maddage R, Mlynarik V, Gruetter R (2009) On the origin of the MR image phase contrast: an in vivo MR microscopy study of the rat brain at 14.1 T. Neuroimage 46(2):345–352
57. Sun H, Wilman AH (2015) Quantitative susceptibility mapping using single-shot echo-planar imaging. Magn Reson Med 73(5):1932–1938
58. Mehdorn HM, Goebel S, Falk D, Volkmann J, Leplow B, Pinsker MO (2008) Deep brain stimulation for movement disorders and its neuropsychological implications. Acta Neurochir Suppl 101:9–12
59. Ilyas A, Pizarro D, Romeo AK, Riley KO, Pati S (2019) The centromedian nucleus: anatomy, physiology, and clinical implications. J Clin Neurosci Off J Neurosurg Soc Aust 63:1–7
60. Gross RE, Krack P, Rodriguez-Oroz MC, Rezai AR, Benabid AL (2006) Electrophysiological mapping for the implantation of deep brain stimulators for Parkinson's disease and tremor. Move Disord 21(Suppl 14):S259–S283
61. Hutchison WD, Lozano AM, Davis KD, Saint-Cyr JA, Lang AE, Dostrovsky JO (1994) Differential neuronal activity in segments of globus pallidus in Parkinson's disease patients. Neuroreport 5(12):1533–1537
62. Kringelbach ML, Jenkinson N, Owen SL, Aziz TZ (2007) Translational principles of deep brain stimulation. Nat Rev Neurosci 8(8):623–635
63. Papavassiliou E, Rau G, Heath S et al (2004) Thalamic deep brain stimulation for essential tremor: relation of lead location to outcome. Neurosurgery 54(5):1120–1129
64. Nölte IS, Gerigk L, Al-Zghloul M, Groden C, Kerl HU (2012) Visualization of the internal globus pallidus: sequence and orientation for deep brain stimulation using a standard installation protocol at 3.0 Tesla. Acta Neurochir 154(3):481–494
65. Dormont D, Ricciardi KG, Tandé D et al (2004) Is the subthalamic nucleus hypointense on T2-weighted images? A correlation study using MR imaging and stereotactic atlas data. AJNR Am J Neuroradiol 25(9):1516–1523
66. Starr PA, Vitek JL, DeLong M, Bakay RA (1999) Magnetic resonance imaging-based stereotactic localization of the globus pallidus and subthalamic nucleus. Neurosurgery 44(2):303–313
67. Ashkan K, Blomstedt P, Zrinzo L et al (2007) Variability of the subthalamic nucleus: the case for direct MRI guided targeting. Br J Neurosurg 21(2):197–200
68. Sharma VD, Mewes K, Wichmann T, Buetefisch C, Willie JT, DeLong M (2017) Deep brain stimulation of the centromedian thalamic nucleus for essential tremor: a case report. Acta Neurochir 159(5):789–793
69. Chan DT, Zhu XL, Yeung JH et al (2009) Complications of deep brain stimulation: a collective review. Asian J Surg 32(4):258–263
70. Fenoy AJ, Schiess MC (2018) Comparison of tractography-assisted to atlas-based targeting for deep brain stimulation in essential tremor. Move Disord Off J Mov Disord Soc 33(12):1895–1901
71. Schweser F, Deistung A, Lehr BW, Reichenbach JR (2010) Differentiation between diamagnetic and paramagnetic cerebral lesions based on magnetic susceptibility mapping. Med Phys 37(10):5165–5178
72. Lemaire JJ, Sakka L, Ouchchane L, Caire F, Gabrillargues J, Bonny JM (2010) Anatomy of the human thalamus based on spontaneous contrast and microscopic voxels in high-field magnetic resonance imaging. Neurosurgery 66:161–172
73. Kanowski M, Voges J, Tempelmann C (2010) Delineation of the nucleus centre median by proton density weighted magnetic resonance imaging at 3 T. Oper Neurosurg (Hagerstown) 66:ons-E121-ons-E3
74. Bender B, Mänz C, Korn A, Nägele T, Klose U (2011) Optimized 3D magnetization-prepared rapid acquisition of gradient echo: identification of thalamus substructures at 3T. AJNR Am J Neuroradiol 32(11):2110–2115
75. Alkemade A, de Hollander G, Keuken MC et al (2017) Comparison of T2*-weighted and QSM contrasts in Parkinson's disease to visualize the STN with MRI. PLoS One 12(4):e0176130
76. Zhang Y, Wei H, Cronin MJ, He N, Yan F, Liu C (2018) Longitudinal atlas for normative human brain development and aging over the lifespan using quantitative susceptibility mapping. Neuroimage 171:176–189
77. Liu T, Eskreis-Winkler S, Schweitzer AD et al (2013) Improved subthalamic nucleus depiction with quantitative susceptibility mapping. Radiology 269(1):216–223
78. Wang Y, Spincemaille P, Liu Z et al (2017) Clinical quantitative susceptibility mapping (QSM): biometal imaging and its emerging roles in patient care. J Magn Reson Imaging 46(4):951–971
79. Sherwin BB (2000) Mild cognitive impairment: potential pharmacological treatment options. J Am Geriatr Soc 48(4):431–441
80. Liu C, Li W, Tong KA, Yeom KW, Kuzminski S (2015) Susceptibility-weighted imaging and quantitative susceptibility mapping in the brain. J Magn Reson Imaging 42(1):23–41
81. Jahn H (2013) Memory loss in Alzheimer's disease. Dialogues Clin Neurosci 15(4):445–454
82. Albert MS, DeKosky ST, Dickson D et al (2011) The diagnosis of mild cognitive impairment due to Alzheimer's disease: recommendations from the National Institute on Aging-Alzheimer's Association workgroups on diagnostic guidelines for Alzheimer's disease. Alzheimers Dementia 7(3):270–279
83. Dubois B, Feldman HH, Jacova C et al (2014) Advancing research diagnostic criteria for Alzheimer's disease: the IWG-2 criteria. Lancet Neurol 13(6):614–629
84. Sisodia SS, Price DL (1995) Role of the β-amyloid protein in Alzheimer's disease. FASEB J 9(5):366–370
85. Everett J, Céspedes E, Shelford LR et al (2014) Evidence of redox-active iron formation following aggregation of ferrihydrite and the Alzheimer's disease peptide β-amyloid. Inorg Chem 53(6):2803–2809
86. Rose SE, Janke AL, Chalk JB (2008) Gray and white matter changes in Alzheimer's disease: a diffusion tensor imaging study. J Magn Reson Imaging 27(1):20–26
87. Benilova I, Karran E, De Strooper B (2012) The toxic Aβ oligomer and Alzheimer's disease: an emperor in need of clothes. Nat Neurosci 15(3):349–357
88. Acosta-Cabronero J, Betts MJ, Cardenas-Blanco A, Yang S, Nestor PJ (2016) In vivo MRI mapping of brain iron deposition across the adult lifespan. J Neurosci 36(2):364–374
89. Hardy JA, Higgins GA (1992) Alzheimer's disease: the amyloid cascade hypothesis. Science 256(5054):184–186
90. Ayton S, Faux NG, Bush AI (2015) Ferritin levels in the cerebrospinal fluid predict Alzheimer's disease outcomes and are regulated by APOE. Nat Commun 6:6760
91. Tiepolt S, Schäfer A, Rullmann M et al (2018) Quantitative susceptibility mapping of amyloid-β aggregates in Alzheimer's disease with 7T MR. J Alzheimers Dis 64(2):393–404
92. Gong NJ, Dibb R, Bulk M, van der Weerd L, Liu C (2019) Imaging beta amyloid aggregation and iron accumulation in Alzheimer's disease using quantitative susceptibility mapping MRI. Neuroimage 191:176–185
93. Eskreis-Winkler S, Zhang Y, Zhang J et al (2017) The clinical utility of QSM: disease diagnosis, medical management, and surgical planning. NMR Biomed 30(4):e3668
94. Zheng W, Nichol H, Liu S, Cheng YC, Haacke EM (2013) Measuring iron in the brain using quantitative susceptibility mapping and X-ray fluorescence imaging. Neuroimage 78:68–74
95. Deistung A, Schäfer A, Schweser F, Biedermann U, Turner R, Reichenbach JR (2013) Toward in vivo histology: a comparison of quantitative susceptibility mapping (QSM) with magnitude-, phase-, and R2*-imaging at ultra-high magnetic field strength. Neuroimage 65:299–314
96. Tolosa E, Gaig C, Santamaria J, Compta Y (2014) Non-motor symptoms in the early motor stages of Parkinson's disease. non-motor symptoms of Parkinson's disease. Oxford University Press, Oxford, pp 24–43
97. Murakami Y, Kakeda S, Watanabe K et al (2015) Usefulness of quantitative susceptibility mapping for the diagnosis of Parkinson disease. AJNR Am J Neuroradiol 36(6):1102–1108
98. Hare D, Ayton S, Bush A, Lei P (2013) A delicate balance: iron metabolism and diseases of the brain. Front Aging Neurosci 5:34
99. Stefanis L (2012) α-Synuclein in Parkinson's disease. Cold Spring Harbor Perspect Med. 2(2):a009399
100. Ahlskog JE (2003) Parkinson's disease: is the initial treatment established? Curr Neurol Neurosci Rep 3(4):289–295

101. Aarsland D, Zaccai J, Brayne C (2005) A systematic review of prevalence studies of dementia in Parkinson's disease. Mov Disord 20(10):1255–1263
102. Davis TL, Kwong KK, Weisskoff RM, Rosen BR (1998) Calibrated functional MRI: mapping the dynamics of oxidative metabolism. Proc Natl Acad Sci U S A 95(4):1834–1839
103. Du G, Lewis MM, Styner M et al (2011) Combined R2* and diffusion tensor imaging changes in the substantia nigra in Parkinson's disease. Move Disord Off J Mov Disord Soc 26(9):1627–1632
104. Golbe LI (2014) Progressive supranuclear palsy. Semin Neurol 34(2):151–159
105. Armstrong MJ (2018) Progressive supranuclear palsy: an update. Curr Neurol Neurosci Rep 18(3):12
106. Hughes AJ, Daniel SE, Kilford L, Lees AJ (1992) Accuracy of clinical diagnosis of idiopathic Parkinson's disease: a clinico-pathological study of 100 cases. J Neurol Neurosurg Psychiatry 55(3):181–184
107. Calloni SF, Conte G, Sbaraini S et al (2018) Multiparametric MR imaging of Parkinsonisms at 3 tesla: Its role in the differentiation of idiopathic Parkinson's disease versus atypical Parkinsonian disorders. Eur J Radiol 109:95–100
108. Petersen RC, Doody R, Kurz A et al (2001) Current concepts in mild cognitive impairment. Arch Neurol 58(12):1985–1992
109. Liu C, Li W, Johnson GA, Wu B (2011) High-field (9.4 T) MRI of brain dysmyelination by quantitative mapping of magnetic susceptibility. Neuroimage 56(3):930–938
110. Litvan I, Agid Y, Calne D et al (1996) Clinical research criteria for the diagnosis of progressive supranuclear palsy (Steele-Richardson-Olszewski syndrome): report of the NINDS-SPSP international workshop. Neurology 47(1):1–9
111. Bartzokis G (2004) Age-related myelin breakdown: a developmental model of cognitive decline and Alzheimer's disease. Neurobiol Aging 25(1):5–18
112. Pitt D, Boster A, Pei W et al (2010) Imaging cortical lesions in multiple sclerosis with ultra–high-field magnetic resonance imaging. Arch Neurol 67(7):812–818
113. Zhang Y, Gauthier SA, Gupta A et al (2016) Magnetic susceptibility from quantitative susceptibility mapping can differentiate new enhancing from nonenhancing multiple sclerosis lesions without gadolinium injection. AJNR Am J Neuroradiol 37(10):1794–1799
114. Tan H, Liu T, Wu Y et al (2014) Evaluation of iron content in human cerebral cavernous malformation using quantitative susceptibility mapping. Invest Radiol 49(7):498–504
115. Hare DJ, Adlard PA, Doble PA, Finkelstein DI (2013) Metallobiology of 1-methyl-4-phenyl-1,2,3,6-tetrahydropyridine neurotoxicity. Metallomics Integr Biomet Sci 5(2):91–109
116. Zhang J, Liu T, Gupta A, Spincemaille P, Nguyen TD, Wang Y (2015) Quantitative mapping of cerebral metabolic rate of oxygen (CMRO2) using quantitative susceptibility mapping (QSM). Magn Reson Med 74(4):945–952
117. Liu T, Spincemaille P, de Rochefort L, Wong R, Prince M, Wang Y (2010) Unambiguous identification of superparamagnetic iron oxide particles through quantitative susceptibility mapping of the nonlinear response to magnetic fields. Magn Reson Imaging 28(9):1383–1389
118. Li J, Lin H, Liu T et al (2018) Quantitative susceptibility mapping (QSM) minimizes interference from cellular pathology in R2* estimation of liver iron concentration. J Magn Reson Imaging 48(4):1069–1079
119. Liu T, Surapaneni K, Lou M, Cheng L, Spincemaille P, Wang Y (2012) Cerebral microbleeds: burden assessment by using quantitative susceptibility mapping. Radiology 262(1):269–278
120. Bandettini PA, Wong EC, Hinks RS, Tikofsky RS, Hyde JS (1992) Time course EPI of human brain function during task activation. Magn Reson Med 25(2):390–397
121. Kim HG, Park S, Rhee HY et al (2017) Quantitative susceptibility mapping to evaluate the early stage of Alzheimer's disease. Neuroimage Clinical 16:429–438
122. Li D, Liu Y, Zeng X et al (2020) Quantitative study of the changes in cerebral blood flow and iron deposition during progression of Alzheimer's disease. J Alzheimers Dis 78(1):439–452
123. Au CKF, Abrigo J, Liu C et al (2021) Quantitative susceptibility mapping of the hippocampal fimbria in Alzheimer's disease. J Magn Reson Imaging 53(6):1823–1832
124. Shahmaei V, Faeghi F, Mohammdbeigi A, Hashemi H, Ashrafi F (2019) Evaluation of iron deposition in brain basal ganglia of patients with Parkinson's disease using quantitative susceptibility mapping. Eur J Radiol Open 6:169–174
125. Au CKF, Abrigo J, Liu C et al (2021) Quantitative susceptibility mapping of the hippocampal fimbria in Alzheimer's disease. J Magn Reson Imaging 53(6):1823–1832
126. Cogswell PM, Wiste HJ, Senjem ML, Gunter JL, Weigand SD, Schwarz CG et al (2021) Associations of quantitative susceptibility mapping with Alzheimer's disease clinical and imaging markers. Neuroimage 224:117433
127. Fedeli MP, Contarino VE, Siggillino S et al (2020) Iron deposition in Parkinsonisms: a quantitative susceptibility mapping study in the deep grey matter. Eur J Radiol 133:109394
128. Ide S, Kakeda S, Ueda I et al (2015) Internal structures of the globus pallidus in patients with Parkinson's disease: evaluation with quantitative susceptibility mapping (QSM). Eur Radiol 25(3):710–718
129. Li DT, Hui ES, Chan Q et al (2018) Quantitative susceptibility mapping as an indicator of subcortical and limbic iron abnormality in Parkinson's disease with dementia. Neuroimage Clin 20:365–373
130. Li J, Li Y, Gutierrez L et al (2020) Imaging the centromedian thalamic nucleus using quantitative susceptibility mapping. Front Hum Neurosci 13:447
131. Li X, Chen L, Kutten K et al (2019) Multi-atlas tool for automated segmentation of brain gray matter nuclei and quantification of their magnetic susceptibility. Neuroimage 191:337–349
132. Li Y, Sethi SK, Zhang C et al (2021) Iron content in deep gray matter as a function of age using quantitative susceptibility mapping: a multicenter study. Front Neurosci 14:1389
133. Moon Y, Han S-H, Moon W-J (2016) Patterns of brain iron accumulation in vascular dementia and Alzheimers Dementia using quantitative susceptibility mapping imaging. J Alzheimers Dis 51(3):737–745
134. Pu R, Wu Z, Yu W et al (2020) The association of myelination in the internal capsule with iron deposition in the basal ganglia in macaques: a magnetic resonance imaging study. Quant Imaging Med Surg 10(7):1526
135. Spotorno N, Acosta-Cabronero J, Stomrud E et al (2020) Relationship between cortical iron and tau aggregation in Alzheimer's disease. Brain 143(5):1341–1349
136. Syam K (2021) Quantitative estimation of regional brain iron deposition-a potential biomarker for Parkinson's Disease and other neurodegenerative conditions causing a typical Parkinsonism. SCTIMST
137. Barber TW, Brockway JA, Higgins LS (1970) The density of tissues in and about the head. Acta Neurol Scand 46(1):85–92
138. Denk C, Torres EH, MacKay A, Rauscher A (2011) The influence of white matter fibre orientation on MR signal phase and decay. NMR Biomed 24(3):246–252
139. Spincemaille P, Anderson J, Wu G et al (2020) Quantitative susceptibility mapping: MRI at 7T versus 3T. J Neuroimaging 30(1):65–75
140. Wei H, Zhang Y, Gibbs E, Chen NK, Wang N, Liu C (2017) Joint 2D and 3D phase processing for quantitative susceptibility mapping: application to 2D echo-planar imaging. NMR Biomed 30(4):e3501
141. Meineke J, Wenzel F, De Marco M et al (2018) Motion artifacts in standard clinical setting obscure disease-specific differences in quantitative susceptibility mapping. Phys Med Biol 63(14):14
142. Kan H, Uchida Y, Arai N et al (2020) Simultaneous voxel-based magnetic susceptibility and morphometry analysis using magnetization-prepared spoiled turbo multiple gradient echo. NMR Biomed 33(5):e4272

Publisher's Note